analytical chemistry

pubs.acs.org/ac Article

SARS-CoV-2 Point-of-Care (POC) Diagnosis Based on Commercial Pregnancy Test Strips and a Palm-Size Microfluidic Device

Meiting Yang, Yidan Tang, Lijuan Qi, Sicai Zhang, Yichen Liu, Baiyang Lu, Jiaxue Yu, Kun Zhu, Bingling Li,* and Yan Du*

Cite This: *Anal. Chem.* 2021, 93, 11956–11964 Read Online

ACCESS | Metrics & More | Article Recommendations | Supporting Information

ABSTRACT: Coronavirus diseases such as the coronavirus disease 2019 (COVID-19) pandemic, caused by severe acute respiratory syndrome coronavirus 2 (SARS-CoV-2), pose serious threats. Portable and accurate nucleic acid detection is still an urgent need to achieve on-site virus screening and timely infection control. Herein, we have developed an on-site, semiautomatic detection system, aiming at simultaneously overcoming the shortcomings suffered by various commercially available assays, such as low accuracy, poor portability, instrument dependency, and labor intensity. Ultrasensitive isothermal amplification [i.e., reverse transcription loop-mediated isothermal amplification (RT-LAMP)] was applied to generate intensified SARS-CoV-2 RNA signals, which were then transduced to portable commercial pregnancy test strips (PTSs) via ultraspecific human chorionic gonadotropin (hCG)-conjugated toehold-mediated strand exchange (TMSE) probes (hCG-P). The entire detection was integrated into a four-channel, palm-size microfluidic device, named the microfluidic point-of-care (POC) diagnosis system based on the PTS (MPSP) detection system. It provides rapid, cost-effective, and sensitive detection, of which the lowest concentration of detection was 0.5 copy/μL of SARS-CoV-2 RNA, regardless of the presence of other similar viruses, even highly similar severe acute respiratory syndrome coronavirus (SARS-CoV). The successful detection of the authentic samples from different resources evaluated the practical application. The commercial PTS provides a colorimetric visible signal, which is instrument- and optimization-free. Therefore, this MPSP system can be immediately used for SARS-CoV-2 emergency detection, and it is worthy of further optimization to achieve full automation and detection for other infectious diseases.

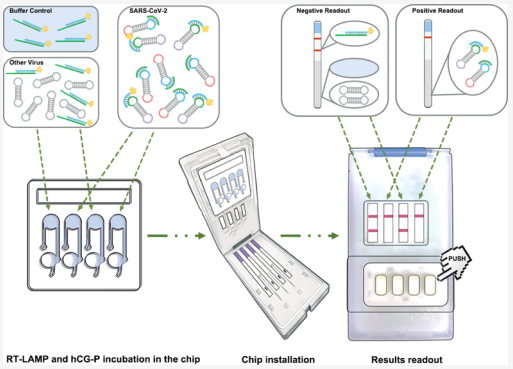

The aggressive spread of severe acute respiratory syndrome coronavirus 2 (SARS-CoV-2) has caused an unprecedented worldwide pandemic.[1] The World Health Organization (WHO) and Centers for Disease Control and Prevention (CDCs) of most countries (e.g. Chinese and American centers) all suggest molecular assays[2,3] as early diagnosis of coronavirus disease 2019 (COVID-19) to limit viral spread and to slow down disease progression.[4,5] Researchers have developed rapid assays based on real-time reverse transcriptase-polymerase chain reaction (RT-PCR), as it is the gold standard for virus detection.[1,6−8] However, expensive equipment, the highly demanding detection environment, and highly skilled personnel are essential for RT-PCR tests, making on-site RT-PCR-based COVID-19 diagnosis impractical for primary cares, especially in developing countries and backward areas.[4,9,10] Furthermore, a time-consuming PCR process and frequent false-negative/positive results limit its diagnostic efficiency in such severe outbreak with continually increasing test demands.[4,11] To overcome these shortcomings, alternative diagnosis methods have been developed, for example, reverse transcription loop-mediated isothermal amplification (RT-LAMP),[12−15] reverse transcription-recombinase polymerase amplification (RT-RPA),[16,17] and reverse-transcription recombinase-aided amplification (RT-RAA)[18−23] coupled with clustered regularly interspaced short palindromic repeats (CRISPR)-based tests.[24−32]

Among these novel methods, recent advancements of RT-LAMP assays make it possible to achieve rapid and easy-to-read assays for COVID-19 diagnosis.[29,33−37] However, most of these assays are based on traditional LAMP and yield naked eye-visible outputs via real-time turbidity monitoring[35] or colorimetric change.[29,33,34,36,37] Due to the general defaults in the amplification principle, nonspecific probes, and limited choice of signaling outputs, these RT-LAMP detections have suffered nonignorable shortcomings such as low sensitivity, frequent misreporting, and low portability.[38] It is still an urgent

Received: April 29, 2021
Accepted: August 9, 2021
Published: August 23, 2021

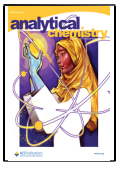

Scheme 1. Diagrammatic Illustration of the Easy-To-See PTS Assay for SARS-Cov-2[a]

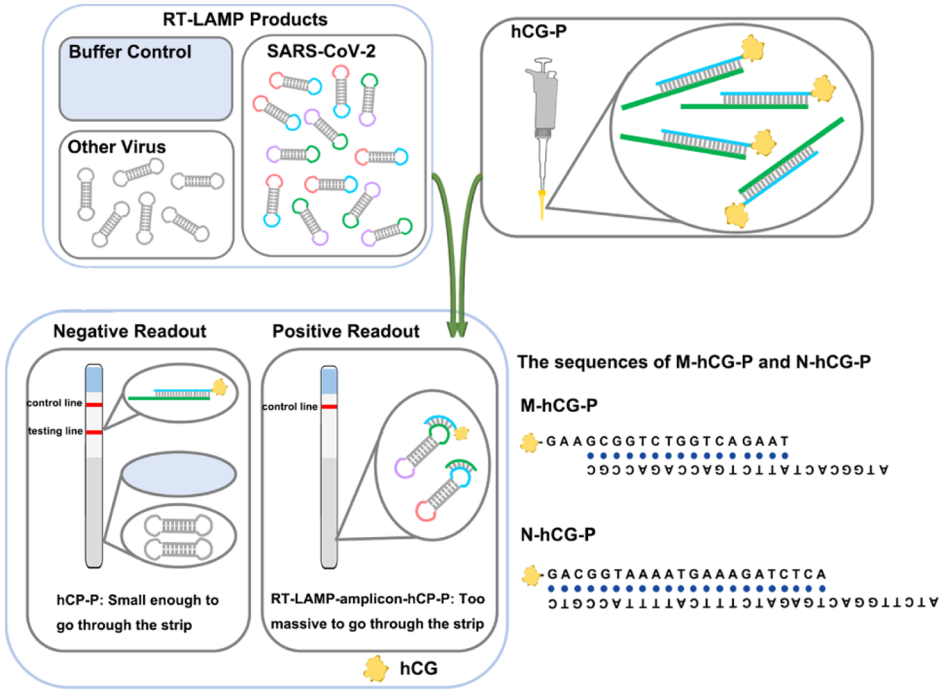

[a]M and N represent the glycoprotein gene and the nucleocapsid protein gene of SARS-CoV-2, respectively.

Scheme 2. Detection Procedure of SARS-Cov-2 Using PTSs and the Portable Microfluidic POC Device; (i) Add Sample Lysis and Mix With the Preloaded RT-LAMP Master Mix in the Chip; (ii) Incubate the Microfluidic-Chip in a Microfluidic Heating Block at 58 °C for 1 h; (iii) Add hCG-Ps and Leave the Chip at 25 °C for 30 min; (iv) Install the Chip Into the POC Device and Close the Lid while Waiting; (v) Press the Chambers on the Device to Infiltrate the Reaction Liquid Into PTSs and Wait for 5 min[a]

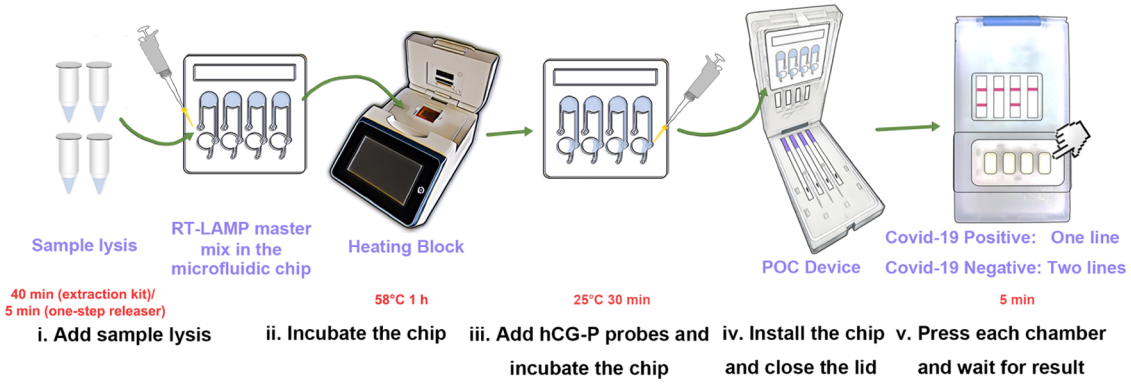

[a]The "yes or no" visible results will clearly appear on PTSs.

need to develop a detection method which could achieve ultrasensitivity, accuracy, and portability simultaneously.

Our previous study has proposed the off-the-shelf pregnancy test strip (PTS), which was originally designed to perform human chorionic gonadotropin (hCG)-responsive analysis, for the detection of DNA targets.[39] Here, for the first time, we developed an efficient and promising solution by transducing ultrasensitive RT-LAMP of SARS-CoV-2 RNA to commercial PTSs via programmable hCG-conjugated toehold-mediated strand exchange (TMSE) probes (hCG-Ps, Scheme 1). The RT-LAMP reaction provides ultrasensitivity by 10^9−10^{10} amplification, and the TMSE probe guarantees high accuracy by sequence-specific recognition, while the PTS generates an instrument-free and plug-in readout that can be observed using naked eyes. Compared with any other lateral flow dipstick (LFD) assays which have to be fabricated according to target sequences, using the PTS as a general signal output can reduce the labor cost and failure risk to a large degree. In order to enhance the portability, the whole transduction process was finally integrated into a rationally designed, four-channel microfluidic point-of-care (POC) device. Following a detailed detection procedure shown in Scheme 2, this so-called microfluidic POC diagnosis system based on the PTS (shortened as MPSP) detection system provides an on-site semiautomated way to detect the target gene. This system has been successfully applied to detect M or N genes of SARS-CoV-2, with ultrasensitivity as high as 0.5 copy/μL, and neither nonrelevant genes nor highly similar severe acute respiratory

https://doi.org/10.1021/acs.analchem.1c01829
Anal. Chem. 2021, 93, 11956−11964

syndrome coronavirus (SARS-CoV) sequences would cause interference. Even importantly, the PTS and microfluidic device facilitate the portable and easy-to-read detection, meanwhile avoiding contamination from aerosol. Possessing such high performance and practicability, the MPSP detection system provides a ready-to-use method for SARS-CoV-2 emergency detection. We believe that the detection of other infectious diseases is expected to be achieved through this system with deeper optimization as well as automation.

EXPERIMENTAL SECTION

Chemicals and Materials. BG-GLA-NHS, all enzymes, and related buffers were obtained from New England Biolabs (Ipswich, MA, USA), unless otherwise indicated. The Amicon Ultra-2 mL 10 K centrifugal filter was obtained from Millipore Inc. (Billerica, MA, USA). NAP-5 desalting columns for purification of oligonucleotides, Ni sepharose HP for affinity purification of the hCG-SNAP fusion protein (human chorionic gonadotropin-O6-alkylguanineDNA alkyltransferase), and prepacked high trap Q columns for hCG-oligo probe purification were bought from GE Life Sciences (Pittsburgh, PA, USA). All other chemicals and solvents were purchased from Sigma-Aldrich, Inc. (St. Louis, MO, USA). The one-step nucleic acid releaser was obtained from Goodwe Biotechnology Taizhou Co., Ltd. (Taizhou, China). The Nûby urine pregnancy test strips (Luv n' care, Ltd., Monroe, LA, USA) were obtained from JD.com (www.jd.com). All oligonucleotides used in this study were synthesized by Sangon Biotec. Co. Ltd., (Shanghai, China), and the sequences are listed in Table S1 (in Supporting Information). The concentrations of DNA/RNA suspensions of oligonucleotides were measured by UV spectrophotometry using a NanoDrop 1000 spectrophotometer (Thermo Scientific, Wilmington, DE, USA).

The authentic reference samples used for the N assay referred to the N gene-containing pseudo-typed virus (PTVN), which were obtained from Zhengzhou Bioyuan Biotech Co. Ltd (Zhengzhou, China). The clinical swab sample (a certified reference sample) of SARS-CoV-2 from a COVID-19 positive patient used for the M assay and 16 negative samples of different viruses (certified reference samples, see details in Supporting Information) including middle east respiratory syndrome coronavirus (MERS-CoV) were obtained from the National Reference Panel for 2019-nCoV Nucleic Acids Detection Kit (National Institutes for Food and Drug Control, Beijing, China). The viral RNA molecules were extracted with the TIANamp virus RNA kit (TIANGEN Biotec. Co. Ltd., Beijing, China) according to the standard protocol. The concentration of SARS-Cov-2 RNA was 3×10^5 copies/mL as quantitated by digital PCR. All these reference samples were diluted with RNase-free H_2O to desired concentrations before use.

Construction of the Recombinant Plasmids. The full-length M gene, the partial sequence of the N gene of SARS-CoV-2 (Genbank Accession MN908947), the full-length M gene, and the partial sequences of the N gene of SARS-CoV (Genbank Accession NC_004718.3) were synthesized by Sangon Biotec Co. Ltd., (Shanghai, China) and constructed into a pUC57 vector. All the recombinant plasmids were dissolved in 1 × TE buffer at a concentration of 2×10^{10} copies/μL and stored at −80 °C until further use.

In Vitro Transcription and Purification. Purified linear, double-stranded DNA templates containing the T7 promoter were transcribed using a MEGAshortscript kit (Thermo Scientific, Wilmington, DE, USA) according to the manufacturer's instructions. The transcription products were incubated with 1 μL of Turbo DNase at 37 °C for 30 min to degrade DNA templates and then purified by polyacrylamide gel RNA purification. All the RNA templates were dissolved with RNase-free H_2O and stored at −80 °C until further use.

RT-LAMP Primer and TMSE Probe Design. Relatively conserved genomic regions in the M and N genes of SARS-CoV-2 were chosen as targets for primer design. RT-LAMP primers were generated using Primer Explorer V5 LAMP primer design software (Eiken Chemical Co., Tokyo, Japan). Each primer set has a pair of outer primers F3 and B3 and a pair of inner primers FIP and BIP as well as a loop primer (LP). Primer specificity was further assessed with NCBI BLAST (https://blast.ncbi.nlm.nih.gov/Blast.cgi). TMSE sequences were designed with the nucleic acid circuit software NUPACK (http://www.nupack.org/).

Expression and Purification of the hCG-SNAP Fusion Protein. The plasmids of the hCGα gene and hCGβ-SNAP-His fusion gene were transfected at a 1:1 ratio into HEK293T cells (Fuheng Biotech.Co., Ltd., Shanghai, China) with PEI 25K (Polysciences, Inc, Warrington, PA, USA) according to the manufacturer's instructions. After 48 h, the cell culture supernatant was collected, purified with Ni sepharose HP, and further desalted and concentrated with the Amicon Ultra-2 mL 10 K centrifugal filter.

Synthesis and Purification of hCG Oligonucleotides. Benzylguanine (BG) was individually conjugated to the amine-functionalized strands via BG-GLA-NHS as previously reported and stored at −20 °C for further use. To prepare hCG-oligonucleotides (hCG-F1), BG-conjugated oligonucleotides were combined with the purified hCGβ-SNAP fusion protein in a 1:2.5 molar ratio in 1 × PBS buffer (8.1 mM Na_2HPO_4, 1.76 mM KH_2PO_4, 136.89 mM NaCl, and 2.67 mM KCl, pH 7.4) and incubated at room temperature (25 °C) for 20 h. After being purified via fast protein liquid chromatography (FPLC), the 1:1 conjugated hCG-F1 probes were concentrated using the Amicon Ultra-2 mL 10 K centrifugal filter. Then, the purification efficacy was confirmed with Coomassie blue staining.

RT-LAMP Assay. Each individual M-RT-LAMP assay was assembled in 20 μL of the reaction mixture containing 1× isothermal amplification buffer (20 mM Tris HCl, 10 mM $(NH_4)_2SO_4$, 50 mM KCl, 2 mM $MgSO_4$, and 0.1% Tween 20, pH 8.8) supplemented with 0.6 μM F3/B3 primers, 2.4 μM FIP/BIP primers, 1.2 μM loop primers, 1.12 mM dNTP, 0.2 M betaine, 2 mM additional $MgSO_4$, 9.6 units of Bst 2.0 DNA polymerase, and 5 units of Warmstart RTx reverse transcriptase. Each individual N-RT-LAMP assay was assembled in 20 μL of the reaction mixture containing 1× isothermal amplification buffer supplemented with 0.6 μM F3/B3 primers, 2.4 μM FIP/BIP primers, 1.2 μM loop primers, 1.12 mM dNTP, 0.6 M betaine, 2 mM additional $MgSO_4$, 9.6 units of Bst 2.0 DNA polymerase, and 3.75 units of Warmstart RTx reverse transcriptase. The total mixture components of the LAMP reaction were similar to that of the RT-LAMP reaction except for adding Warmstart RTx reverse transcriptase. Reactions were subjected to isothermal amplification at 58 °C for 60 min. Amplicons were testified with agarose gel electrophoresis and imaged with a blue light gel imager (Sangon Biotec Co. Ltd., Shanghai, China).

https://doi.org/10.1021/acs.analchem.1c01829
Anal. Chem. 2021, 93, 11956−11964

Easy-To-See Test Strip Assay. For preparing hCG-P, 20 nM of M-hCG-F1 (or N-hCG-F1) and its partial complementary strand (M-R or N-R) were incubated at room temperature for 1 h. Then, 15 μL of the corresponding concentration of M-hCG-P (or N-hCG-P) probes was mixed with 15 μL of M-RT-LAMP (or N-RT-LAMP) products for the corresponding time at 25 °C. Subsequently, 20 μL of 1 × PBS was added to the mixture, and the PTSs were dipped into the reaction. Pictures were taken after 2 min with a smart phone (iPhone 11 Pro Max, Apple, CA, USA).

Development of the Microfluidic Chip and the POC Device. The microfluidic chip (Proteinbiosen Biotec. Co. Ltd., Beijing, China) equipped with amplification zones was originally designed for nucleic acid amplification. To make the chip fit our assay, additional incubation zones and a set of pressure-vent holes below the amplification zone were fabricated on this chip. The designed POC device is shown in Figure S1 (in Supporting Information).

Data Analysis. The analysis of relative intensities was quantified with Adobe Photoshop CC (Adobe Systems Incorporated, CA, USA) and ImageJ. Detailed methods were carried out as previously described. The relative intensity of each signal response shown on the PTS was quantified as I [relative intensity] = [intensity of the control band]/[intensity of test band]. ΔI laid below each bar graph was calculated as ΔI = [relative intensity of NC] − [relative intensity of PC]. All the figures were laid out with GraphPad Prism 6 (GraphPad Software, San Diego, CA, USA).

RESULTS AND DISCUSSION

Sensing Principle of the Detection. As is the case with pregnancy tests in general, false positive or false negative results from molecular diagnostics can be extremely impactful. In particular, nucleic acid amplification assays often need to be able to detect samples specifically, in order to discern exactly what variant of a gene or organism is present. We have previously shown rationally adapted so-called oligonucleotide strand displacement (OSD) probes to function in the context of the PTS transduction assay.[39] Herein, hCG is the original target of a commercial PTS, which is self-expressed and covalently conjugated to the antisense sequence of RT-LAMP amplicons. To distinguish the highly homologous SARS-CoV sequences from SARS-CoV-2, several pairs of hCG-labeled TMSE probes (i.e., M-hCG-Ps and N-hCG-Ps) were designed that would be activated by the amplified M and N loop sequences, respectively (Table S1, in Supporting Information). The detection procedure and principle of this assay are shown in Scheme 1. After the hybridization of M-hCG-F1 (or N-hCG-F1) and its partial complementary strand (M-R or N-R), respectively, the specific probes, M-hCG-P (or N-hCG-P), were successfully constructed. Then, the M-hCG-P (or N-hCG-P) probes were incubated with RT-LAMP amplicons of M (or N) genes, respectively, and the hybridization reactions were allowed to proceed for 30 min at 25 °C. The hybridization of the hCG-P to the correct loop products of LAMP was initiated at the toehold domain and then proceeded via branch migration and dissociation of the hCG-labeled DNA strand. Subsequently, yes or no results, instantly visible to the naked eyes, were yielded with commercial PTSs. In the presence of the correct gene templates, the RT-LAMP amplicons were produced and hybridized with hCG-Ps, disabling migration of hCG-Ps on the strip due to the huge and massive LAMP amplicons. Thus, there should be only a control line on the strip, indicating SARS-CoV-2 positive readout. On the contrary, amplicons of negative samples [negative control (NC) or other viruses] could not hybridize with hCG-Ps, leaving hCG-Ps to migrate freely on the strip, making both the testing line and control line appear on the strip, which indicates SARS-CoV-2 negative readout.

RT-LAMP Assay for SARS-CoV-2. According to the sensing principle described above, RT-LAMP assay was at first designed to amplify relatively conserved regions targeting the membrane glycoprotein (M) and the nucleocapsid protein (N)genes (GenBank accession MN908947). After optimizing concentrations of betaine, $MgSO_4$, dNTP, primers, and Warmstart RTx reverse transcriptase and reaction temperature of LAMP reactions (Figure S2, in Supporting Information), the LAMP amplicons of the copy number concentration gradients (0.5 to 2000 copies/μL) of M (Figure 1A) or N (Figure 1B)

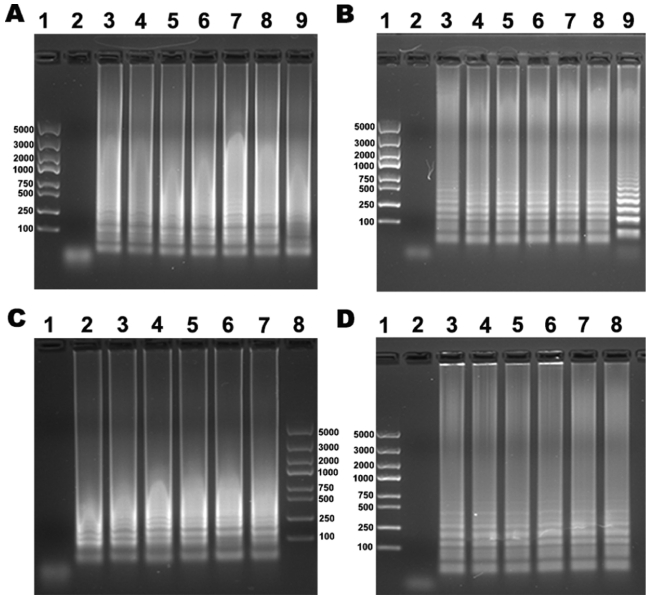

Figure 1. Agarose gel electrophoretic characterization of LAMP or RT-LAMP amplicons of synthetic M DNA (A), N DNA (B), M RNA (C), and N RNA (D) of SARS-CoV-2 or SARS. (A) Lane 1: DNA molecular weight markers; lane 2: nontarget (buffer control); lane 3−8: 0.5, 1, 2, 20, 200, and 2000 copies/μL of M DNA of SARS-CoV-2; lane 9: 2000 copies/μL of M DNA of SARS-CoV. (B) Lane 1: DNA molecular weight markers; lane 2: nontarget (buffer control); lane 3−8: 0.5, 1, 2, 20, 200, and 2000 copies/μL of N DNA of SARS-CoV-2; lane 9: 2000 copies/μL of N DNA of SARS-CoV. (C) Lane 1: nontarget (buffer control); lane 2−7: 0.5, 1, 2, 20, 200, and 2000 copies/μL of M RNA of SARS-CoV-2; lane 8: DNA molecular weight markers. (D) Lane 1: DNA molecular weight markers; lane 2: nontarget (buffer control); lane 3−8: 0.5, 1, 2, 20, 200, and 2000 copies/μL of N RNA of SARS-CoV-2.

DNA templates of SARS-Cov-2 and 2000 copies/μL of M or N templates of SARS-CoV were tested with agarose gel electrophoresis. Then, we examined our RT-LAMP assay for RNA templates of SARS-CoV-2. Figure 1C,D revealed that RT-LAMP for M and N assays could also detect as few as 0.5 copy/μL of M and N RNA templates, respectively. These results demonstrated that such RT-LAMP assay was capable of rapid amplification of SARS-CoV-2 targets and reduction of the detection limit. Note that the bands of amplicons could be observed in the presence of both synthetic DNA and RNA targets of SARS-CoV-2 and SARS-CoV because of the high

https://doi.org/10.1021/acs.analchem.1c01829
Anal. Chem. 2021, 93, 11956−11964

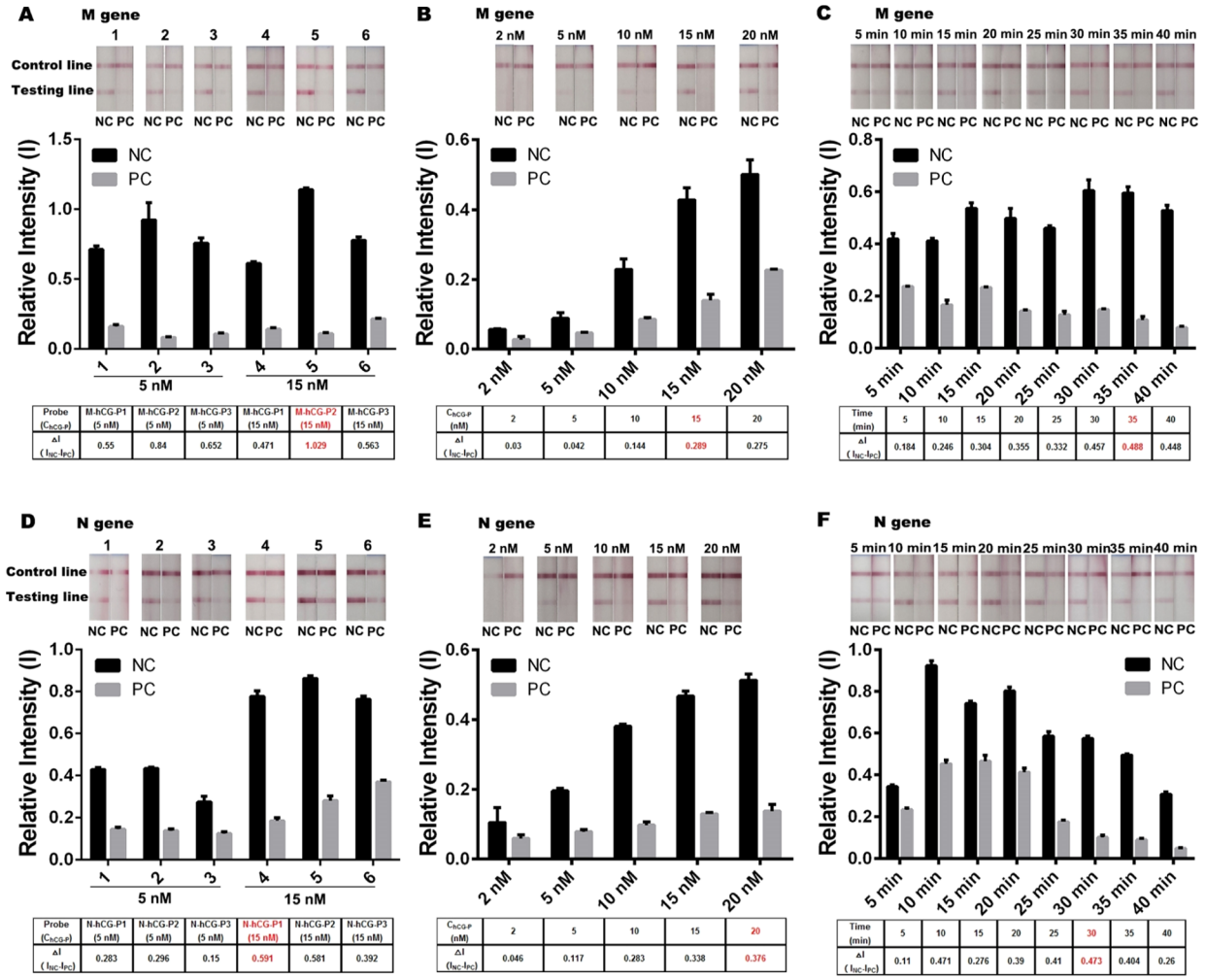

Figure 2. Optimization of M-hCG-P and N-hCG-P. (A) Determination of the optimal probe for M gene detection. Lane 1−3: 5 nM M-hCG-P1, M-hCG-P2, and M-hCG-P3 probes; lane 4−6: 15 nM M-hCG-P1, M-hCG-P2, and M-hCG-P3 probes. Optimization of the concentration of the probes (B) and incubation time (C) of RT-LAMP for the M gene with the optimal M-hCG-P2 probe. (D) Determination of the optimal probe for N gene detection. Lane 1−3: 5 nM N-hCG-P1, N-hCG-P2, and N-hCG-P3 probes; lane 4−6: 15 nM N-hCG-P1, N-hCG-P2, and N-hCG-P3 probes. Optimization of the concentration of the probes (E) and incubation time (F) of RT-LAMP for the N gene with the optimal N-hCG-P1 probe. The bar graphs below the test strip pictures respectively present the color intensity of the lines on the test strips quantified with ImageJ software.

homology of these two coronaviruses. Also, the amplified bands showed only a little difference between SARS-CoV-2 and SARS-CoV, indicating the lack of specificity of traditional gel electrophoresis characterization.[40]

DNA Conjugation to the hCG-SNAP Fusion Protein. In order to implement this general strategy for PTS-based gene detection, we needed the expression of the hCG-SNAP fusion protein to site-specifically conjugate DNA to hCG. The conjugation method followed our previous paper[39] and was verified using protein tagging technology (Figure S3, in Supporting Information). The expression of the hCG-SNAP fusion protein was first verified by western blot (Figure S3A, in Supporting Information) and the commercial PTSs (Figure S3B, in Supporting Information), indicating the good protein activity and its ability to bind PTSs. The conjugation of the oligonucleotide (M-F1 or N-F1) to the hCG-SNAP fusion protein and its purification using anion exchange chromatography were further confirmed by SDS−PAGE (Figure S3C,D, in Supporting Information). These results showed that the hCG-DNA conjugates had obvious band shifts compared to the hCG-SNAP fusion protein and the FPLC purification could efficiently eliminate unlabeled fusions.

Optimization of the Specific TMSE Probe and Determination of the Easy-To-See PTS Assay. To implement our purpose, some important optimizations of the experimental conditions were first investigated. Three sets of hCG-P (i.e., M/N-hCG-P1, M/N-hCG-P2, and M/N-hCG-P3) were designed for M and N genes, respectively. As shown in Figure 2A,D, M-hCG-P2 and N-hCG-P1 generated strongest signals than other ones. Thus, we selected M-hCG-P2 and N-hCG-P1 as the optimal hCG probes. Furthermore, the concentration of the probes (Figure 2B,E) and incubation time (Figure 2C,F) were also optimized. It is determined that 15 nM M-hCG-P2 and 35 min of hybridization time were the optimal conditions for M target detection, while 20 nM N-hCG-P1 and 30 min of hybridization time were the optimal conditions for N target detection. Under these optimized conditions, tests with serial dilutions of synthetic DNA/RNA targets were performed to determine the sensitivity of our PTS assay. As shown in Figure 3, our strategy could detect as low as

https://doi.org/10.1021/acs.analchem.1c01829
Anal. Chem. 2021, 93, 11956−11964

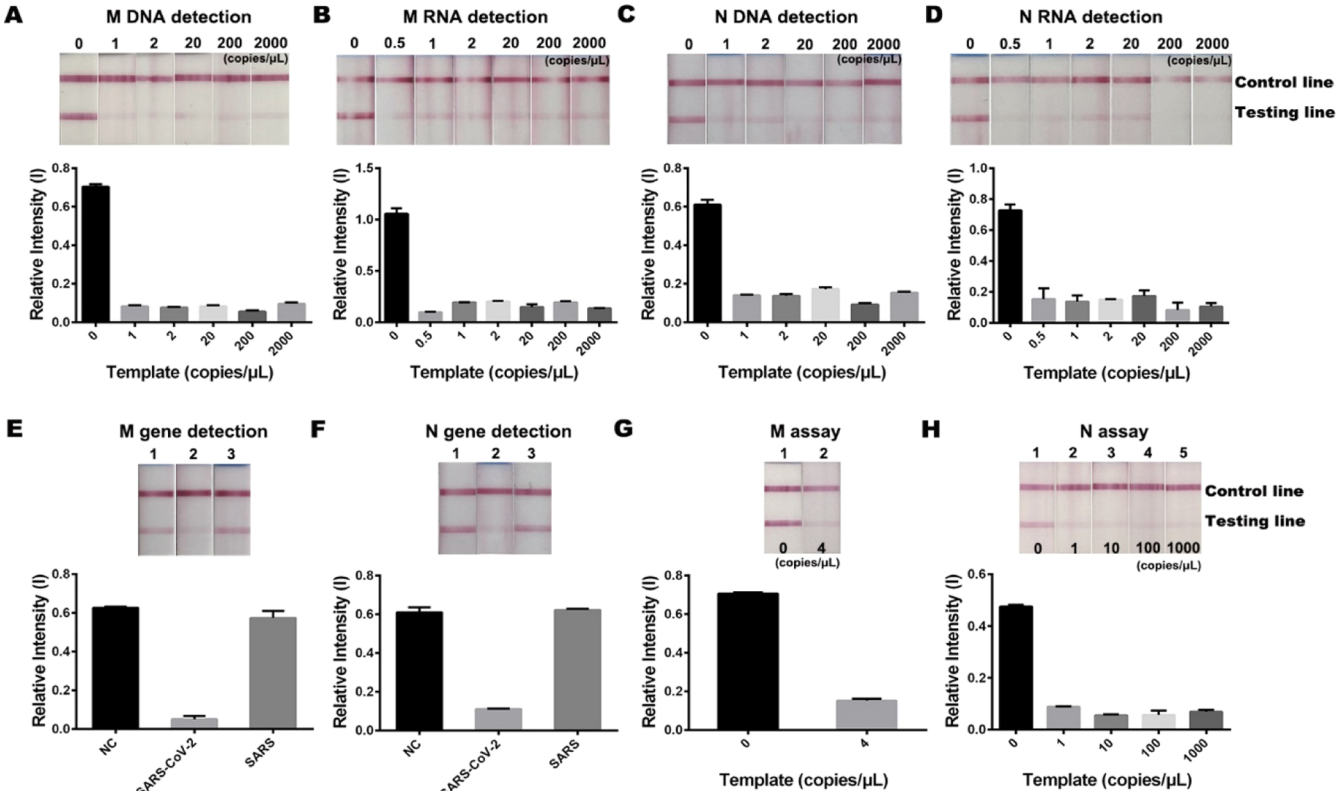

Figure 3. Sensitive and specific detection of SARS-CoV-2 using LAMP (or RT-LAMP) to hCG transduction. The determination of sensitivity of (A) M DNA templates via the M assay; (B) M RNA templates via the M assay; (C) N DNA templates via the N assay; and (D) N RNA templates via the N assay. The determination of specificity of (E) M assay and (F) N assay for SARS-CoV-2. (E) Strip-1: NC; strip-2: 2000 copies/μL of M DNA of SARS-CoV-2; strip-3: 2000 copies/μL of M DNA of SARS-CoV. (F) Strip-1: NC; strip-2: 2000 copies/μL of N DNA of SARS-CoV-2; strip-3: 2000 copies/μL of N DNA of SARS-CoV. Real sample detection of the M assay (G) and N assay (H). (G) Strip-1: NC; strip 2: 4 copies/μL of clinical swab sample of SARS-CoV-2 from the National Reference Panel. (H) Strip-1: NC; strip 2−5: 1, 10, 100, and 1000 copies/μL of N gene samples of SARS-CoV-2 from PTVNs. All the bar graphs below the test strip pictures, respectively, presented the color intensity of the lines on the test strips quantified with ImageJ software.

1 copy/μL of the M or N DNA templates (Figure 3A,C) and 0.5 copy/μL of M or N RNA templates (Figure 3B,D), being lower than most of the reported RT-LAMP reactions (Table S2, in Supporting Information). These results showed the extreme high sensitivity of our assay. In contrast, we respectively implemented negative control (NC, buffer control) and 2000 copies/μL of M or N genes of SARS DNA templates to identify the specificity of our assay. It was demonstrated that only the strips for M (Figure 3E) or N (Figure 3F) templates of SARS-CoV-2 showed the single control line, indicating a positive result, while the strips for SARS templates and the NC ones showed the control line and the testing line, indicating the negative results. These results successfully validated that the hCG-labeled TMSE transduction could accurately distinguish SARS-CoV-2 and SARS-CoV gene sequences in LAMP amplicons with a high signal amplitude.

Authentic Sample Detection. Authentic samples from different resources were tested for further evaluation of our assay. Clinical swab samples derived from patients with SARS-CoV-2, provided within the National Reference Panel, were used for the M assay detection. The M assay showed a positive result in the detection of 4 copies/μL clinical samples (Figure 3G). Samples for the N assay detection were pseudotyped viral particles containing the full length of the N gene of SARS-CoV-2. The N gene samples with different copy number concentrations, ranging from 1 to 1000 copies/μL, were tested by the N assay. Figure 3H shows that as low as 1 copy/μL of PTVNs could be detected without any loss in signal intensity. We also investigated the clinical selectivity of the M assay and N assay. The buffer control and 16 types of viruses (i.e., certified reference samples, see details in Figure S4, in Supporting Information) were tested with our MPSP detection system, and no positive signal (only a red control line) was observed for either M or N assay. These results suggest that no cross-reaction occurs in our MPSP system with other pathogenic microorganisms. To comply with the POC test request, the RNA of PTVNs was extracted by a one-step nucleic acid releaser, which only costs around 5 min in contrast to 40 min of the regular RNA extraction method, but showed almost the same positive signal (Figure S5, in Supporting Information). This indicates the adequateness of our method as a POC test.

Combination of the PTS Assay with the Microfluidic Device (The MPSP Assay). The POC diagnostics of SARS-CoV-2 is realized through the amalgamation of a microfluidic chip and a portable POC device, which process has been shortened as MPSP. The microfluidic chip was designed for four-channel reaction, which was perfectly fit for our assay. There were two zones and three pressure-vent pores in each channel of the chip. The amplification zones, preloaded with the RT-LAMP master mix, were where isothermal amplification happens. The incubation zones were designed for adding hCG-Ps after amplification (Figure 4A,B). The portable POC

https://doi.org/10.1021/acs.analchem.1c01829
Anal. Chem. 2021, 93, 11956−11964

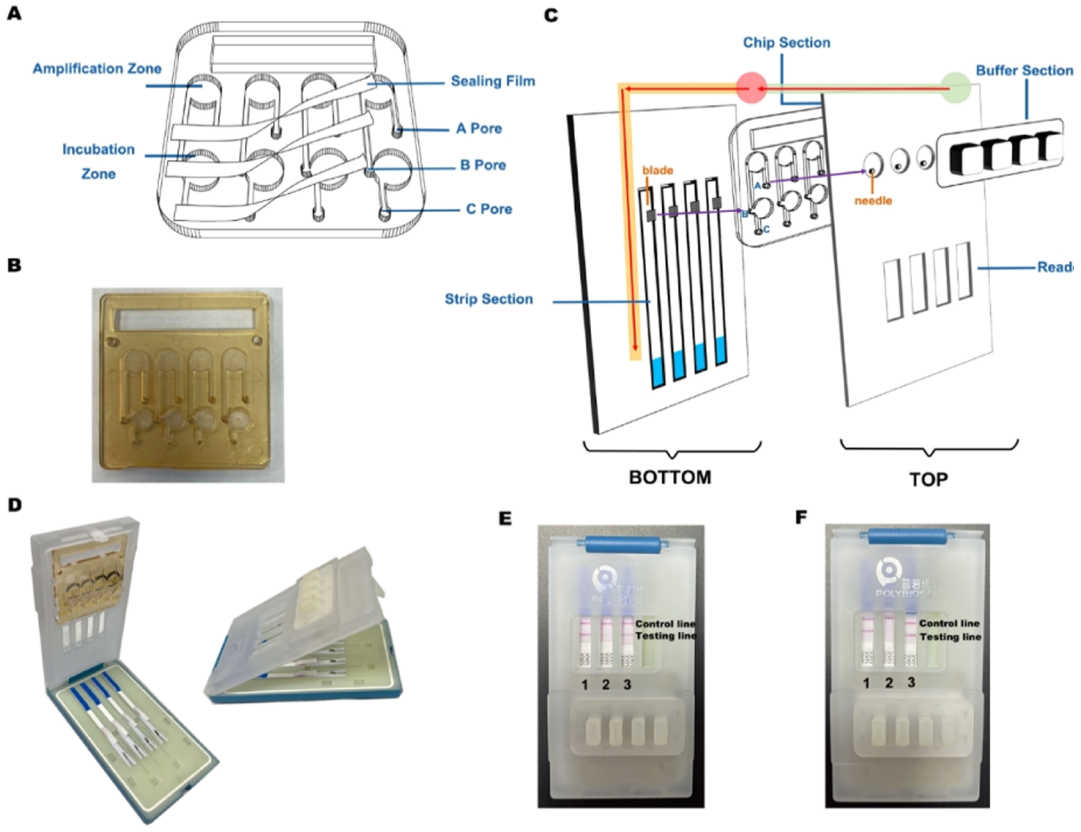

Figure 4. Detection of authentic samples using the microfluidic POC device. (A−D) Structure illustration and actual items of the microfluidic POC device. (A) Structure of the microfluidic chip. (B) Actual microfluidic chip. (C) Different units of the portable POC device. Arrows in red represent the liquid flow direction in the device. (D) Actual POC device. Detection of authentic samples from different sources via the M assay (E) and the N assay (F) with the MPSP. (E) Strip-1: NC; strip-2: 4 copies/μL of clinical samples of SARS-CoV-2 from the National Reference Panel; strip-3: 120 copies/μL of clinical samples of MERS-CoV from National Reference Panel. (F) Strip-1: NC; strip-2: 1000 copies/μL of N gene samples of SARS-CoV-2 from PTVNs; strip-3: 120 copies/μL of clinical samples of MERS-CoV.

device (Figures 4C and S1, in Supporting Information), composed of the top and bottom parts, perfectly accommodated the microfluidic chip to accomplish the multichannel detection via PTSs. Four subdivisions endow the whole device with semiautomation and user-friendliness (Figure 4C,D): (1) the chip section, where the microfluidic chip should be installed, is on the inner side of the lid. The A pores on the microfluidic chip will be punctured by the four needles fixed on the lid to interconnect the fluid in the buffer section and amplification zone in the chip. (2) The buffer section locates on the upside of the lid and contains four soft chambers, each preloaded with 25 μL of 1 × PBS. (3) The strip section refers to the four-channel detection area located at the bottom, where the PTSs are installed. There are also four miniblades in the strip section, which will puncture the B pores upon closure of the device to interconnect the fluid in the incubation zone in the chip and the strip section. (4) The readout section stands for the four transparent windows that allow signal reading on the PTSs without opening the lid.

The whole MPSP assay could accomplish rapid diagnosis for COVID-19 simply through the following steps (Scheme 2): (i) the sample lysis was injected into the amplification zone via A pores, where the RT-LAMP master mix was preadded. The microfluidic chip was sealed with three pieces of the sealing film. (ii) The microfluidic chip was later heated on a matching instrument to execute RT-LAMP, and after RT-LAMP, the chip was placed at room temperature. (iii) The B and C pores were unsealed before the injection of hCG-Ps via B pores, and the liquid in the amplification zone and incubation zone was mixed by pipetting via the B pores. Subsequently, all pores were sealed, and the chip was incubated at room temperature for 30 min. (iv) The microfluidic chip was then installed in the chip section of the device, with A and B pores punctured by the needles on the lid and the blades in the strip section, respectively. Thus, the total liquid could flow smoothly from the buffer section to the amplification zone in the chip and then to the test strips in the strip section. (v) After applying pressure to the chambers in the buffer section, 1 × PBS flowed through the interconnected pores, until a well-mixed status of the amplicons and the probes reaches the PTSs in the strip section, which would give a yes or no result in a few minutes on the transparent window of the readout section.

The successful detection of the clinical samples of SARS-CoV-2 with the MERS-CoV samples for comparison was realized by the M assay (Figure 4E). The detection results for the PTVNs using the N assay with the clinical samples of MERS for comparison are displayed in Figure 4F. Only a control line emerged in the middle of the PTSs, which implies the positive result, but the additional presence of the test line signifies the negative readouts for NC and MERS-CoV samples. Our assay expedites the simple and reliable diagnosis for COVID-19 with high specificity and sensitivity. The derived device is expected to vitalize the poorly equipped laboratories after being developed into a high-throughput POC

https://doi.org/10.1021/acs.analchem.1c01829
Anal. Chem. 2021, 93, 11956−11964

tool for application in clinical diagnosis and contribute to possible constraints in disease control.

CONCLUSIONS

In summary, we developed a portable POC prototype MPSP detection system that could yield rapid ready-to-use colorimetric SARS-CoV-2 diagnosis. The system integrates the high sensitivity powered by the RT-LAMP reaction, high specificity provided by TMSE, optimization/fabrication-free commercial pregnancy strip readout, and the user-friendly interface granted by the microfluidic chip and POC device. It requires neither a laboratory environment nor an expensive PCR instrument to achieve on-site SARS-CoV-2 molecular diagnosis. The time consumed throughout the entire assay, starting with the treatment of the clinical sample by the one-step nucleic acid releaser, is only less than 2 h. Each test is as cheap as 2 dollars. In addition, our system offers semiautomated multichannel detection, which could, with certain modification and improvement, evolve into a high-throughput automated virus diagnostic system that offers on-site detection of multiple viruses, including, but not limited to, SARS-CoV-2.

ASSOCIATED CONTENT

Supporting Information

The Supporting Information is available free of charge at https://pubs.acs.org/doi/10.1021/acs.analchem.1c01829.

Real-time fluorescence LAMP; cell culture; immunoblotting; structure illustration of the POC device; optimization of the reaction system of LAMP; preparation and purification of hCG-F1; specific detection of SARS-CoV-2; diagnostic result for PTVNs by the one-step nucleic acid releaser; related sequences of RT-LAMP and hCG-Ps; and related articles for SARS-CoV-2 detection with the isothermal amplification method (PDF).

AUTHOR INFORMATION

Corresponding Authors

Bingling Li − *State Key Laboratory of Electroanalytical Chemistry, Changchun Institute of Applied Chemistry, Chinese Academy of Sciences, Changchun 130022 Jilin, P. R. China; Department of Chemistry, University of Science & Technology of China, Hefei 230026 Anhui, China*; Email: binglingli@ciac.ac.cn

Yan Du − *State Key Laboratory of Electroanalytical Chemistry, Changchun Institute of Applied Chemistry, Chinese Academy of Sciences, Changchun 130022 Jilin, P. R. China; Department of Chemistry, University of Science & Technology of China, Hefei 230026 Anhui, China*; orcid.org/0000-0003-3197-7204; Email: duyan@ciac.ac.cn, duyan.bessie@gmail.com

Authors

Meiting Yang − *State Key Laboratory of Electroanalytical Chemistry, Changchun Institute of Applied Chemistry, Chinese Academy of Sciences, Changchun 130022 Jilin, P. R. China*

Yidan Tang − *State Key Laboratory of Electroanalytical Chemistry, Changchun Institute of Applied Chemistry, Chinese Academy of Sciences, Changchun 130022 Jilin, P. R. China*

Lijuan Qi − *State Key Laboratory of Electroanalytical Chemistry, Changchun Institute of Applied Chemistry, Chinese Academy of Sciences, Changchun 130022 Jilin, P. R. China; Department of Chemistry, University of Science & Technology of China, Hefei 230026 Anhui, China*

Sicai Zhang − *State Key Laboratory of Electroanalytical Chemistry, Changchun Institute of Applied Chemistry, Chinese Academy of Sciences, Changchun 130022 Jilin, P. R. China*

Yichen Liu − *State Key Laboratory of Electroanalytical Chemistry, Changchun Institute of Applied Chemistry, Chinese Academy of Sciences, Changchun 130022 Jilin, P. R. China; Department of Chemistry, University of Science & Technology of China, Hefei 230026 Anhui, China*

Baiyang Lu − *State Key Laboratory of Electroanalytical Chemistry, Changchun Institute of Applied Chemistry, Chinese Academy of Sciences, Changchun 130022 Jilin, P. R. China*

Jiaxue Yu − *State Key Laboratory of Electroanalytical Chemistry, Changchun Institute of Applied Chemistry, Chinese Academy of Sciences, Changchun 130022 Jilin, P. R. China*

Kun Zhu − *Proteinbiosen Biotechnology Limited Liability Company, Beijing 100000, P.R. China*

Complete contact information is available at: https://pubs.acs.org/10.1021/acs.analchem.1c01829

Author Contributions

Y. D. and B.L. conceived the work. M.T.Y. and Y.D. designed and carried out all the experiments for RT-LAMP-PTS transduction. M.T.Y., L.J.Q., and S.C.Z made the hCG-DNA probe. M.T.Y. and Y.D.T. developed the RT-LAMP primers and protocols of LAMP. B.Y.L. and J.X.Y. performed initial experimental validations of LAMP. M.T.Y., Y.D.T., and L.J.Q. designed and tested the loop primers and the hCG-DNA probes. L.J.Q. performed the selectivity test of the clinical samples. K. Z. developed the POC prototype and the microfluidic chip. M.T.Y. and Y.C.L improved the microfluidic chip. Y.D., M.T.Y., and B.L. wrote the manuscript.

Notes

The authors declare no competing financial interest.
Patents were applied for PTS assay (no. 202110159269.4) and the microfluidic POC device (no. 202110046585.0).

ACKNOWLEDGMENTS

This work is dedicated to the 90th birthday of Professor Shaojun Dong in the Changchun Institute of Applied Chemistry, Chinese Academy of Science. This work is financially supported by the National Natural Science Foundation of China (grant numbers 21874129, 22004118, and 22174137), the National Key R&D Program of China (2019YFC1905400), the New coronavirus (COVID-19) emergency project of Jilin Province (20200901022SF), and the International Technological Cooperation Project of Jilin Scientific and Technological Development Program (grant number 20200801044GH).

REFERENCES

(1) Pan, Y.; Long, L.; Zhang, D.; Yuan, T.; Cui, S.; Yang, P.; Wang, Q.; Ren, S. *Clin. Chem.* **2020**, *66*, 794−801.
(2) Binnicker, M. J. *Clin. Chem.* **2020**, *66*, 664−666.

(3) Holshue, M. L.; DeBolt, C.; Lindquist, S.; Lofy, K. H.; Wiesman, J.; Bruce, H.; Spitters, C.; Ericson, K.; Wilkerson, S.; Tural, A.; Diaz, G.; Cohn, A.; Fox, L.; Patel, A.; Gerber, S. I.; Kim, L.; Tong, S.; Lu, X.; Lindstrom, S.; Pallansch, M. A.; Weldon, W. C.; Biggs, H. M.; Uyeki, T. M.; Pillai, S. K.; Washington State-nCo, VCIT.. *N. Engl. J. Med.* **2020**, *382*, 929−936.
(4) Feng, W.; Newbigging, A. M.; Le, C.; Pang, B.; Peng, H.; Cao, Y.; Wu, J.; Abbas, G.; Song, J.; Wang, D.-B.; Cui, M.; Tao, J.; Tyrrell, D. L.; Zhang, X.-E.; Zhang, H.; Le, X. C. *Anal. Chem.* **2020**, *92*, 10196−10209.
(5) Li, C.; Ren, L. *Transboundary Emerging Dis.* **2020**, *67*, 1485−1491.
(6) Corman, V. M.; Landt, O.; Kaiser, M.; Molenkamp, R.; Meijer, A.; Chu, D. K.; Bleicker, T.; Brünink, S.; Schneider, J.; Schmidt, M. L.; Mulders, D. G.; Haagmans, B. L.; van der Veer, B.; van den Brink, S.; Wijsman, L.; Goderski, G.; Romette, J.-L.; Ellis, J.; Zambon, M.; Peiris, M.; Goossens, H.; Reusken, C.; Koopmans, M. P.; Drosten, C. *Euro Surveill.* **2020**, *25*, 2000045−2000053.
(7) Chu, D. K. W.; Pan, Y.; Cheng, S. M. S.; Hui, K. P. Y.; Krishnan, P.; Liu, Y.; Ng, D. Y. M.; Wan, C. K. C.; Yang, P.; Wang, Q.; Peiris, M.; Poon, L. L. M. *Clin. Chem.* **2020**, *66*, 549−555.
(8) Hirotsu, Y.; Mochizuki, H.; Omata, M. *J. Virol. Methods* **2020**, *284*, 113926−113931.
(9) Yelin, I.; Aharony, N.; Tamar, E. S.; Argoetti, A.; Messer, E.; Berenbaum, D.; Shafran, E.; Kuzli, A.; Gandali, N.; Shkedi, O. *Clin Infect Dis.* **2020**, *71*, 2073−2078.
(10) Zhao, Y.; Chen, F.; Li, Q.; Wang, L.; Fan, C. *Chem. Rev.* **2015**, *115*, 12491−12545.
(11) Augustine, R.; Hasan, A.; Das, S.; Ahmed, R.; Mori, Y.; Notomi, T.; Kevadiya, B.; Thakor, A. *Biology* **2020**, *9*, 182−198.
(12) Kashir, J.; Yaqinuddin, A. *Med. Hypotheses* **2020**, *141*, 109786.
(13) Barnes, D. G.; Vidiassov, M.; Ruthensteiner, B.; Fluke, C. J.; Quayle, M. R.; McHenry, C. R. *PLoS One* **2013**, *8*, No. e69446.
(14) Shen, M.; Zhou, Y.; Ye, J.; Abdullah Al-Maskri, A. A.; Kang, Y.; Zeng, S.; Cai, S. *J. Pharm. Anal.* **2020**, *10*, 97−101.
(15) Nagamine, K.; Hase, T.; Notomi, T. *Mol. Cell. Probes* **2002**, *16*, 223−229.
(16) Qian, J.; Boswell, S. A.; Chidley, C.; Lu, Z. X.; Pettit, M. E.; Gaudio, B. L.; Fajnzylber, J. M.; Ingram, R. T.; Ward, R. H.; Li, J. Z.; Springer, M. *Nat. Commun.* **2020**, *11*, 5920.
(17) Piepenburg, O.; Williams, C. H.; Stemple, D. L.; Armes, N. A. *PLoS Biol.* **2006**, *4*, No. e204.
(18) Xue, G.; Li, S.; Zhang, W.; Du, B.; Cui, J.; Yan, C.; Huang, L.; Chen, L.; Zhao, L.; Sun, Y.; Li, N.; Zhao, H.; Feng, Y.; Wang, Z.; Liu, S.; Zhang, Q.; Xie, X.; Liu, D.; Yao, H.; Yuan, J. *Anal. Chem.* **2020**, *92*, 9699−9705.
(19) Wang, R.-h.; Zhang, H.; Zhang, Y.; Li, X.-n.; Shen, X.-x.; Qi, J.-j.; Fan, G.-h.; Xiang, X.-y.; Zhan, Z.-f.; Chen, Z.-w.; Ma, X.-j. *Virol. J.* **2019**, *16*, 86−94.
(20) Qi, J.; Li, X.; Zhang, Y.; Shen, X.; Song, G.; Pan, J.; Fan, T.; Wang, R.; Li, L.; Ma, X. *Arch. Virol.* **2019**, *164*, 1843−1850.
(21) Fan, G. H.; Shen, X. X.; Li, F.; Li, X. N.; Bai, X. D.; Zhang, R. Q.; Wang, R. H.; Lei, W. W.; Wang, H. Y.; Ma, X. J.; Wu, G. Z. *Biomed. Environ. Sci.* **2019**, *32*, 926−929.
(22) Zhang, X.; Guo, L.; Ma, R.; Cong, L.; Wu, Z.; Wei, Y.; Xue, S.; Zheng, W.; Tang, S. *J. Microbiol. Methods* **2017**, *139*, 202−204.
(23) Shen, X.-x.; Qiu, F.-z.; Shen, L.-P.; Yan, T.-f.; Zhao, M.-c.; Qi, J.-J.; Chen, C.; Zhao, L.; Wang, L.; Feng, Z.-s.; Ma, X.-j. *BMC Infect. Dis.* **2019**, *19*, 229−233.
(24) Lucia, C.; Federico, P.-B.; Alejandra, G. C. *bioRxiv* **2020**, DOI: 10.1101/2020.02.29.971127.
(25) Joung, J.; Ladha, A.; Saito, M.; Segel, M.; Bruneau, R.; Huang, M. W.; Kim, N. G.; Yu, X.; Li, J.; Walker, B. D.; Greninger, A. L.; Jerome, K. R.; Gootenberg, J. S.; Abudayyeh, O. O.; Zhang, F. *medRxiv* **2020**, DOI: 10.1101/2020.05.04.20091231.
(26) Yoshimi, K.; Takeshita, K.; Yamayoshi, S.; Shibumura, S.; Yamauchi, Y.; Yamamoto, M.; Yotsuyanagi, H.; Kawaoka, Y.; Mashimo, T. *medRxiv* **2020**, DOI: 10.1101/2020.06.02.20119875.
(27) Gootenberg, J. S.; Abudayyeh, O. O.; Lee, J. W.; Essletzbichler, P.; Dy, A. J.; Joung, J.; Verdine, V.; Donghia, N.; Daringer, N. M.; Freije, C. A.; Myhrvold, C.; Bhattacharyya, R. P.; Livny, J.; Regev, A.; Koonin, E. V.; Hung, D. T.; Sabeti, P. C.; Collins, J. J.; Zhang, F. *Science* **2017**, *356*, 438−442.
(28) Gootenberg, J. S.; Abudayyeh, O. O.; Kellner, M. J.; Joung, J.; Collins, J. J.; Zhang, F. *Science* **2018**, *360*, 439−444.
(29) Zhang, Y.; Odiwuor, N.; Xiong, J.; Sun, L.; Nyaruaba, R. O.; Wei, H.; Tanner, N. A. *medRxiv* **2020**, DOI: 10.1101/2020.02.26.20028373.
(30) Broughton, J. P.; Deng, X.; Yu, G.; Fasching, C. L.; Servellita, V.; Singh, J.; Miao, X.; Streithorst, J. A.; Granados, A.; Sotomayor-Gonzalez, A.; Zorn, K.; Gopez, A.; Hsu, E.; Gu, W.; Miller, S.; Pan, C.-Y.; Guevara, H.; Wadford, D. A.; Chen, J. S.; Chiu, C. Y. *Nat. Biotechnol.* **2020**, *38*, 870−874.
(31) Jung, S. I.; Kim, M. S.; Jeong, C. W.; Kwak, C.; Hong, S. K.; Kang, S. H.; Joung, J. Y.; Lee, S. H.; Yun, S. J.; Kim, T.-H.; Park, S. W.; Jeon, S. S.; Kang, M.; Lee, J. Y.; Chung, B. H.; Hong, J. H.; Ahn, H.; Kim, C.-S.; Kwon, D. D. *Investig Clin Urol* **2020**, *61*, 19−27.
(32) Pang, B.; Xu, J.; Liu, Y.; Peng, H.; Feng, W.; Cao, Y.; Wu, J.; Xiao, H.; Pabbaraju, K.; Tipples, G.; Joyce, M. A.; Saffran, H. A.; Tyrrell, D. L.; Zhang, H.; Le, X. C. *Anal. Chem.* **2020**, *92*, 16204−16212.
(33) Lamb, L. E.; Bartolone, S. N.; Ward, E.; Chancellor, M. B. *PLoS One* **2020**, *15*, No. e0234682.
(34) L'Helgouach, N.; Champigneux, P.; Schneider, F. S.; Molina, L.; Espeut, J.; Alali, M.; Baptiste, J.; Cardeur, L.; Dubuc, B.; Foulongne, V.; Galtier, F.; Makinson, A.; Marin, G.; Picot, M.-C.; Prieux-Lejeune, A.; Quenot, M.; Robles, F. C.; Salvetat, N.; Vetter, D.; Reynes, J.; Molina, F. *medRxiv* **2020**, DOI: 10.1101/2020.05.30.20117291.
(35) Yan, C.; Cui, J.; Huang, L.; Du, B.; Chen, L.; Xue, G.; Li, S.; Zhang, W.; Zhao, L.; Sun, Y.; Yao, H.; Li, N.; Zhao, H.; Feng, Y.; Liu, S.; Zhang, Q.; Liu, D.; Yuan, J. *Clin. Microbiol. Infect.* **2020**, *26*, 773−779.
(36) Anahtar, M. N.; McGrath, G. E. G.; Rabe, B. A.; Tanner, N. A.; White, B. A.; Lennerz, J. K. M.; Branda, J. A.; Cepko, C. L.; Rosenberg, E. S. *medRxiv* **2020**, DOI: 10.1093/ofid/ofaa631.
(37) Ben-Assa, N.; Naddaf, R.; Gefen, T.; Capucha, T.; Hajjo, H.; Mandelbaum, N.; Elbaum, L.; Rogov, P.; Daniel, K. A.; Kaplan, S.; Rotem, A.; Chowers, M.; Szwarcwort-Cohen, M.; Paul, M.; Geva-Zatorsky, N. *medRxiv* **2020**, DOI: 10.1101/2020.04.22.20072389.
(38) Chen, G.; Chen, R.; Ding, S.; Li, M.; Wang, J.; Zou, J.; Du, F.; Dong, J.; Cui, X.; Huang, X.; Deng, Y.; Tang, Z. *Analyst* **2020**, *145*, 440−444.
(39) Du, Y.; Pothukuchy, A.; Gollihar, J. D.; Nourani, A.; Li, B.; Ellington, A. D. *Angew. Chem., Int. Ed. Engl.* **2017**, *56*, 992−996.
(40) Bhadra, S.; Jiang, Y. S.; Kumar, M. R.; Johnson, R. F.; Hensley, L. E.; Ellington, A. D.; Tzong-Yueh, C. *PloS One* **2015**, *10*, No. e0123126.

https://doi.org/10.1021/acs.analchem.1c01829
Anal. Chem. 2021, 93, 11956−11964